scientific reports

Check for updates

OPEN

Influence of fractal fabric on the shear characteristics of large scale accumulation bodies

Yidan Huang[1,2]✉ & Wentai Chen[1]

Large-scale accumulation bodies composed of loose materials are among the theoretical and practical topics of greatest interest to engineers and scientists. Although accumulation bodies have been widely studied across multiple academic disciplines, the impact of particle materials on mechanical properties remains insufficiently explored. The motivation for this study is to investigate the relationship between the fabric characteristics of large-scale accumulation bodies and their shear mechanical properties, field investigations were conducted to obtain particle size distribution characteristics, which led to determining the fractal dimension *D* as a descriptor of the fabric. For samples with different fractal dimensions, we conducted large direct shear tests and MatDEM numerical simulations. The topological characteristics of the particle contact network during shear were then analysed using a complex network method. The results revealed that the accumulation bodies' shear strength obtained from both the physical and numerical experiments first increased but then decreased with increasing fractal dimension, following a normal distribution with a mean value of 2.5 and an amplification factor that is proportional to the vertical load. The analysis of complex network parameters also has consistent patterns. On the basis of these experimental results, this study investigates the shear mechanical properties of accumulation bodies from both macroscopic and microscopic perspectives, providing deeper insights into the link between macroscopic responses and the mesoscale structure of force chains, explaining the mechanism by which fractal dimensions affect their shear characteristics and providing new evaluation methods for the utilization and stability assessment of large-scale accumulation materials.

Keywords Fractal dimension, Complex network, Accumulation body, Large direct shear, MatDEM

Quaternary large-scale accumulation bodies made of loose materials are widely developed and distributed in mountainous areas. With large volumes and particle sizes, they often cause a series of geological disasters and lead to significant geological issues, seriously threatening human survival, livelihoods, and the safety of construction projects. Large-scale accumulation bodies are a type of geological material distinct from rock and soil, consisting of many discrete particles, such as large blocks and fine-grained soil, that form a complex and disordered system[1]. It has a complex composition and highly uneven arrangements, typical of a granular structure. These characteristics have made them novel and crucial research subjects, garnering extensive attention from soil mechanics and rock mechanics[2]. Scholars worldwide have increasingly studied accumulation bodies, including fabric characteristics[3], dynamic properties[4], self-organizing phenomena[5], stratification[6], failure modes and characteristics[7], deformation evolution mechanisms[8] and stability evaluations of accumulation slopes[9–12]. However, owing to the inherently complex multibody system of accumulations, classical mechanics does not apply to these systems. Consequently, despite extensive research on accumulation bodies by numerous scholars across various fields, a theoretical system and fundamental paradigm have yet to be established, and there is a lack of systematic foundational research on their physical and mechanical properties.

When researching accumulation bodies, whether macroscopically or microscopically, the focus is on redescribing various phenomena, starting from the most basic characteristics and physical laws. Generally, the particle size distribution (PSD) is considered the most basic fabric characteristic and the starting point for analysing various physical and mechanical properties of accumulation bodies. Thus, image parameters are often used to represent the particle size distribution. However, only empirical relationships can be provided when the influence of the particle size distribution is considered if image parameters are used to describe it. As a result,

[1]School of Civil Engineering, Southwest Jiaotong University, Chengdu 610031, China. [2]National Engineering Research Center of Geological Disaster Prevention Technology in Land Transportation, Chengdu 610031, China. ✉email: huangyidan@swjtu.edu.cn

particle size distribution is mostly avoided in many accumulation body studies, and the resulting laws only apply to the specific particle size distribution used in the research.

Existing geotechnical theories still lack a definitive method for describing the internal fabric of large-scale accumulation bodies. There are only simple definitions based on particle size, such as "when the fine-grained soil with a particle size smaller than 0.075 *mm* exceeds 25% of the total mass, it should be named coarse-grained mixed soil"[13]. Chinese official standards such as DLT 5395-2007 and DLT 5016-2011 only provide brief requirements, such as the content of particles smaller than 5 *mm* not exceeding 30% and particles smaller than 0.075 mm not exceeding 5%. Researchers have proposed various distribution functions for the particle size distribution[14–19]. Turcotte first applied the fractal model to geological fragmentation problems and gave a definition of fractal in his pioneering and foundational research, *Fractals and Fragmentation*[20]: "*If the number-size distribution of objects satisfies the condition, then a fractal is defined with a fractal dimension... A power-law relation between number and size is, by definition, a fractal.*" Owing to the universality of fractal laws and their advantages in mathematical and physical foundations, the power-law distribution has become one of the representative particle size distribution functions for accumulation bodies (especially rock piles) and has been widely applied. Chen *et al.*[21] used direct shear tests to study the relationship between the shear strength of soils in Fujian, China, and the fractal dimension and provided the formula $t = a + bD + cD2$ (where D is the fractal dimension, t is the shear strength, and a, b, c are parameters). Through shear tests, Zhang *et al.*[22] reported that the cohesion and friction angle of granite residuals decrease with increasing fractal dimension. Avsar *et al.*[23] conducted uniaxial compression tests on igneous conglomerates. They reported a statistically significant positive correlation between the uniaxial compressive strength and fractal dimension of fragmentation, with a reasonably high correlation coefficient.

In addition, the large-scale accumulation body, a complex system of discrete particles[24,25], manifests macroscopic properties stemming from microscopic interactions between particles. By considering particles as points and their interactions as connections, the accumulation body can be abstracted into a complex network. The characteristics of stress transmission within the accumulation body can be intuitively represented through the particle contact network. Consequently, some researchers have employed complex network methods to investigate the contact network characteristics of granular materials. Walker[26,27] initially proved the feasibility of using complex network theory to study granular systems and explored particle fragmentation through complex network theory, finding that the strong force chains between particles follow the shortest path principle. Tordesillas[28] used complex network techniques to analyse X-ray images from particle shear tests and DEM simulation results and discovered that the position and deformation of the shear band are established early in the loading process before the maximum shear stress is reached. Li Ziqi[29] applied complex network methods to investigate triaxial compression DEM simulations of sandy soil particles, revealing that particle connectivity strengthens with compression, enhancing the force chain transmission capacity. The introduction of complex network methods offers a new perspective for studying accumulation bodies. However, current research on accumulation bodies primarily uses complex network theory combined with numerical simulations to describe phenomena, with few reports incorporating actual physical experiments.

This study explores the relationship between the fabric characteristics of large-scale accumulation bodies and their shear mechanical properties. By field investigating accumulation bodies to obtain particle size distribution characteristics, we chose the fractal dimension D as a parameter to describe the particle fabric. We conducted large direct shear tests with different fractal dimensions D for particles up to 40 mm and established MatDEM direct shear numerical simulations on the basis of field investigation results. By combining complex network methods, we systematically studied the shear mechanical properties of accumulation bodies with different fractal dimensions from macroscopic and microscopic perspectives.

Physical experiments

Field investigation and materials

Large-scale accumulation bodies are widely distributed in the mountainous regions of western China. To assist in the preparation of experimental materials, we selected and investigated seven accumulation bodies located in Caopo, Wenchuan, Aba Tibetan and Qiang Autonomous Prefectures, Sichuan Province, China, along the national highway G317, from K74+775 to K75+740, between Dujiangyan and Wenchuan. The lithology of these accumulation bodies mainly consists of gray and dark gray carbonate rock salts, as shown in Figures 1(a) to 1(f).

We conducted onsite sampling at the seven accumulation body sites and then analysed the samples using a combination of sieving and direct measurement. Each site had a section line set up with three sampling points at the upper, middle, and lower parts, as shown in Figure 2. Seven section lines and 21 sampling points were set up across the seven sites of accumulation bodies.

The mesh sizes of the onsite sieves were 5 mm, 10 mm, 20 mm, 30 mm, and 40 mm. For large rocks that were difficult to sieve, the maximum linear dimensions in three mutually perpendicular directions were measured directly with a ruler. The average particle size and mass of the rocks were then calculated using the following Equation (1) and (2):

$$d = \frac{a+b+c}{3} \tag{1}$$

$$m = \frac{1}{81}\pi d^3 \rho_s \tag{2}$$

In the equation, d represents the average particle size of the rock; a, b, and c represent the maximum linear dimensions in three mutually perpendicular directions of the rock; m represents the average mass of the rock;

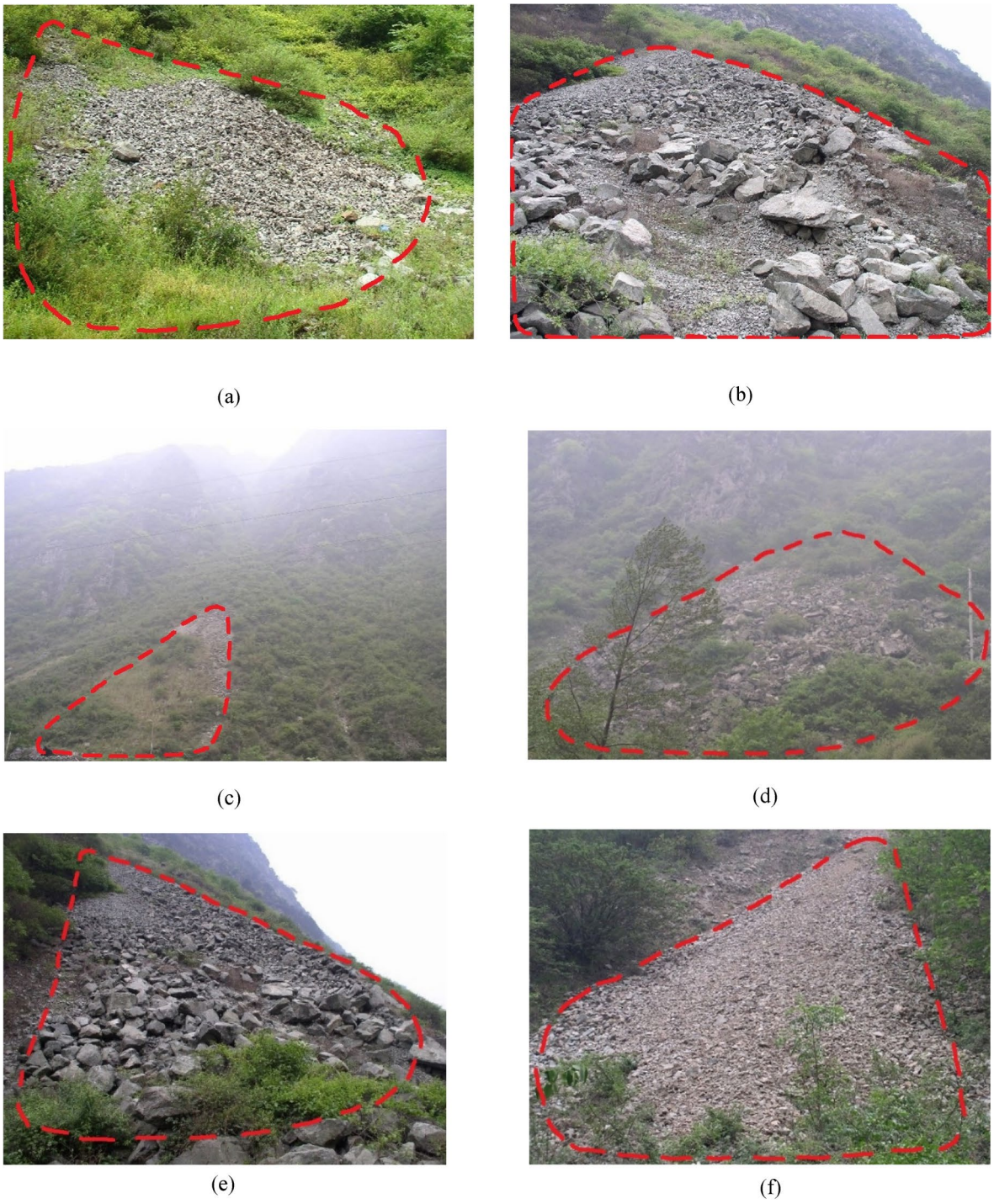

Fig. 1. Field photos of accumulation bodies.

and ρ_s represents the density of the rock. The particle test results were summarized in Supplementary Table S1 online.

Given the wide particle size distribution of the accumulation bodies—where the differences between the maximum and minimum particle sizes often exceed a 100-fold—a fractal description proves to be more suitable. For fractal fitting, the particle size-weight distribution fractal equation proposed by Yang Peiling et al.[30] (Eq. (3)) was employed. The fitting results are presented in Table 1.

$$\frac{W(\delta < \overline{d}_i)}{W_0} = (\frac{\overline{d}_i}{\overline{d}_{\max}})^{3-D} \tag{3}$$

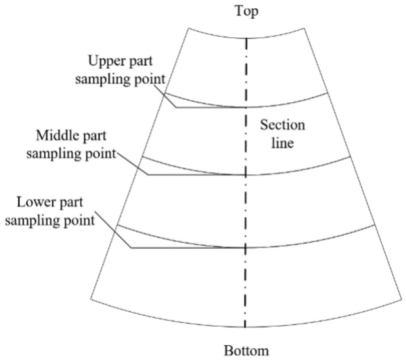

Fig. 2. Diagram of site measurement points layout.

Site No	Fractal Dimension(*D*)			Average particle size($\overline{d}$ /mm)			Correlation Coefficient(R^2)		
	Upper	Middle	Lower	Upper	Middle	Lower	Upper	Middle	Lower
1	2.61	2.52	2.36	170	205	238	0.9562	0.9616	0.9216
2	2.48	2.33	2.25	250	320	314	0.9591	0.9784	0.9552
3	2.59	2.49	2.28	197	209	283	0.9585	0.9493	0.9518
4	2.43	2.31	2.23	255	330	358	0.962	0.9762	0.9721
5	2.43	2.30	2.22	313	349	365	0.966	0.9671	0.9672
6	2.79	2.78	2.76	60	69	73	0.9084	0.9495	0.9287
7	2.48	2.33	2.27	245	268	311	0.9207	0.9499	0.9321

Table 1. Results of particle size fractal analysis at each point.

where $\overline{d}_i$ represents the average diameter between two sieve sizes d_i and d_{i+1},$\overline{d}_{\max}$ denotes the average diameter of the largest soil particles, $W(\delta < \overline{d}_i)$ represents the cumulative weight of soil particles larger than $\overline{d}_i$, and W_0 represents the total weight of soil particles across all size classes.

From Table S1 and 1, we can observe these conclusions:

1. The particle size distributions of the accumulation bodies exhibit apparent regularity along the vertical height direction. The upper part has a higher content of fine particles and fewer coarse particles; the middle part shows an increase in coarse particles, whereas the bottom part consists predominantly of coarse particles with fewer fine particles. The average particle size increases from the upper to the bottom points.
2. The particle size distribution of the accumulation bodies conforms to a fractal distribution, and the fractal dimension can reflect the fabric characteristics of the accumulation bodies. A smaller fractal dimension corresponds to a greater proportion of coarse particles, whereas a larger fractal dimension corresponds to a greater proportion of fine particles. Additionally, the fractal dimension reflects the average size of the particles: a smaller fractal dimension corresponds to a larger average particle size, whereas a larger fractal dimension corresponds to a smaller average particle size.
3. With increasing slope height, the fractal dimension of the accumulation bodies gradually increases, with larger fractal dimensions in the upper part and smaller fractal dimensions in the lower part. The fractal dimensions range between 2 and 3. Specifically, the maximum fractal dimension at the upper points is 2.79, the minimum fractal dimension is 2.43, and the average fractal dimension is 2.55; for the middle points, the fractal dimension is 2.78, 2.30, and 2.44; and for the lower points, the fractal dimension is 2.76, 2.22, and 2.3. The fractal dimensions of the field accumulation bodies range from 2.2 ~ 2.8. Thus, we define our study range as $D = 2.2 \sim 2.8$.

Based on the field investigation results and GB/T 50,123–2019, we set the maximum particle size for this experiment at 40 mm (less than 1/8 ~ 1/10 of the shear box height of 400 mm). Natural accumulations were chosen and initially air-dried for two weeks before transportation to the indoor experimental site. Since this study primarily examines the influence of fractal dimension on shear properties, we minimized moisture-related effects by sieving and air-drying the samples again upon arrival. Samples were then sealed in plastic woven bags for storage, with moisture content verified to remain below 5% before testing. Finally, the samples were sieved and configured into seven different fractal dimension ratios, ranging from 2.2 to 2.8. The particle size distributions and sample configurations for each fractal dimension are shown in Figs. 3 and 4, respectively.

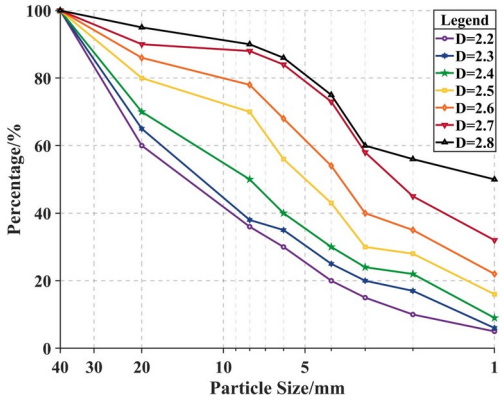

Fig. 3. Particle size distribution diagram of physical experiments.

Equipments and plans

Among the shear characteristics of accumulation bodies, the shear strength and internal friction angle are two key mechanical properties. We conducted large direct shear tests on samples with different fractal dimensions to obtain the shear strength and internal friction angle. Additionally, we carried out static pile sand experiments to supplement the results of the internal friction angle.

Large direct shear test

The large direct shear test was conducted using a DHJ50-2 stacking-type large direct shear device from the Geotechnical Engineering Laboratory at Southwest Jiaotong University. The testing machine solved the problem of the reduction in the shear surface during the test by replacing the upper shear box of the traditional direct shear equipment with eight stacked rings, each 20 mm thick, which significantly expanded the shear zone and greatly reduced the impact of particle breakage. It has a total dimension of *505 mm* (diameter) × *400 mm* (height) and is suitable for samples with a maximum particle size of ≤*60 mm*. The main technical specifications include a gap size of *10 mm* between the upper and lower shear boxes, a maximum vertical load of *700 kN*, a maximum horizontal thrust of *700 kN*, and an automatically controlled shear rate of 0.01~4.8 mm/min. The machine uses four vertical displacement gauges and eleven horizontal displacement gauges to record displacement, with data being collected and processed synchronously by an industrial control computer automatic control system. The equipment is shown in Figure 5.

We weighed enough materials (180 kg in total) for each fractal dimension based on the ratio in Figure 3, divided them evenly into five portions, and filled them into the shear box, compacting each layer by striking with a hammer 50 times to ensure uniform compaction. The total amount of each loading was approximately 155--165 kg, varying with the fractal dimension. After filling, we conducted shear tests under vertical loads of 200 kPa, 500 kPa, and 800 kPa for each fractal dimension. The experiment procedures followed the GB/T 50123-2019 Geotechnical Testing Methods standard, which uses automated control of vertical loads and horizontal thrust, with a shear rate set at 1 mm/min until failure. Computer software automatically recorded shear force–displacement data and plotted curves in real time.

Static sand heap trial

To cross-validate the internal friction angle findings, we included the sand heap trial, which simulates particle accumulation and slope formation in controlled conditions, mirroring natural conditions and complementing the shear test results. The sand heap trial employed the slope rolling accumulation method, which simulates real-world accumulation processes under controlled conditions, ensuring more accurate and reliable results. During the experiment, we set the slope angle, the slope used to roll the particles, to 70° to simulate the natural sliding of the particles during the accumulation process. A glass surface slope was used to minimize frictional effects on the slope.

In the experiment, the particles were scooped with a shovel and then slowly and freely slid down along the glass panel *20 cm* above the top of the heap. When the particle heap reached a critical state, sand deposition was halted, and the angle of repose was measured. The critical heap state[31] is defined as the point where particles slide along the slope where despite continuous vertical accumulation of the heap, its horizontal dimension no longer increases. Upon reaching this state, the particles further accumulate until the vertical height stabilizes, indicating the critical heap state. The angle of inclination α formed at the critical heap state is regarded as the angle of repose of the particles, $\alpha = \arctan(h/r)$, where h is the height of the accumulation and r is the radius of the base of the accumulation. The resulting angle formed at this critical heap state is considered the angle of repose for the particles.

Four experiments were conducted for each fractal dimension specified in Figure 3. In each experiment, particle heaps totaling 40 kg were arranged according to the selected ratio. The height and length of the particle heap were measured in four trials, and the average values were used to calculate the angle of repose. Each heap formed during the experiment was a conical frustum with a base diameter of 60 cm and a height of 20 cm, with a volume of approximately 0.12 m3, as shown in Supplementary Fig. S1 online.

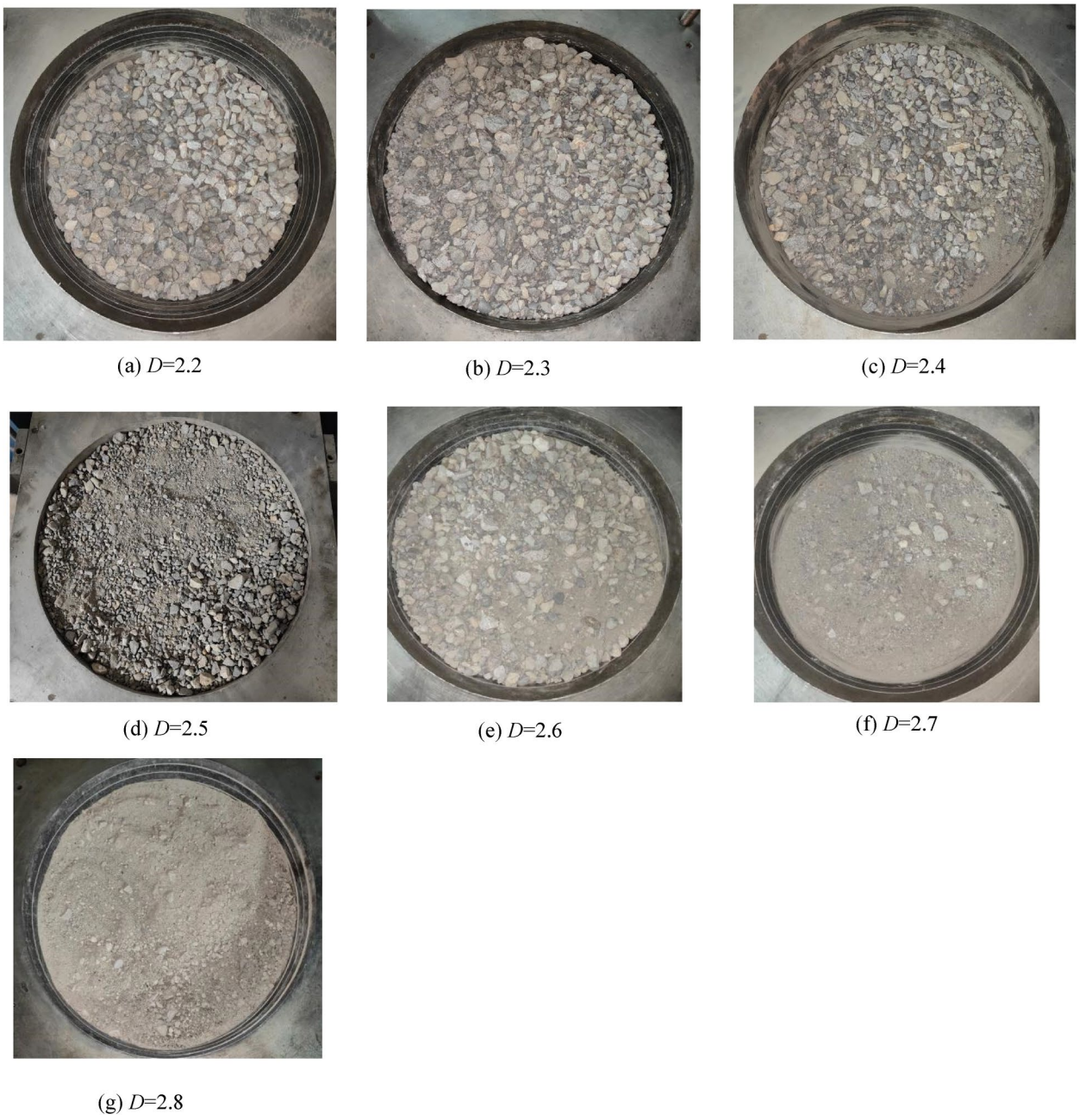

Fig. 4. Samples of accumulation bodies with different fractal dimensions.

Methods

Numerical simulation

Traditional methods, such as finite element analysis based on continuous media, have limitations in studying accumulation bodies. Since Cundall P. A.[32,33] introduced the discrete element method (DEM), this approach has become a prominent tool for analysing granular materials at the microscopic level in geotechnical simulations. MatDEM, a discrete element method numerical simulation software independently developed by Nanjing University, has been applied to simulate a series of problems, such as landslides and rock bursts. MatDEM utilizes GPU-based matrix computation, which enables a 30-fold increase in the number of units processed compared to conventional software, effectively addressing the issue of computational load[34]. Based on this advantage, we have chosen MatDEM as our discrete element numerical simulation software.

Numerical simulation experiments using MatDEM are generally divided into three steps: model building, material assignment, and iterative numerical simulation. The first step is to establish the accumulation model. In terms of particle size, the model is based on physical experiments. Since the upper limit for particle elements in MatDEM software is 1 million, the use of a 1:1 scale for numerical simulation exceeds this limit. Therefore, a scaling ratio of 1:4 was determined through experiments, which balances accuracy and speed. At this ratio, the

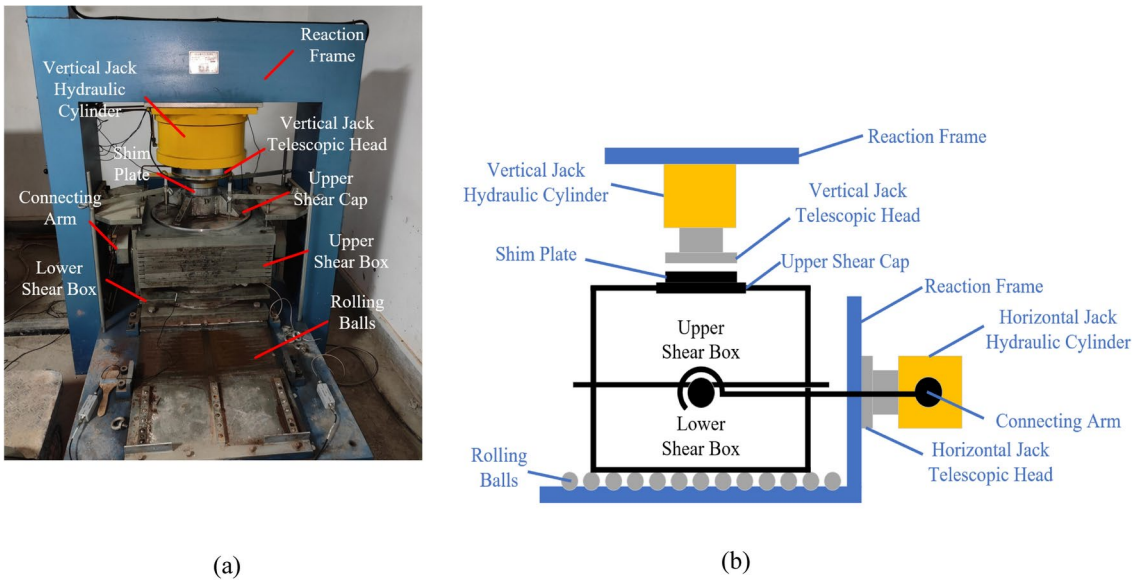

Fig. 5. Diagram of the ring shear test device: (**a**) device frontal view, (**b**) schematic diagram of the device.

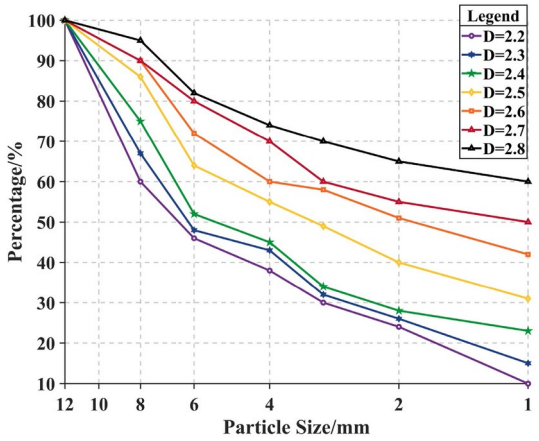

Fig. 6. Particle size distribution diagram of numerical simulation test.

maximum particle diameter is 12 mm. The shear rate is set to 0.5mm/min, a 1:2 scaling ratio compared to the physical experiment, following Froude's law. We adjusted the particle size distribution accordingly, and the PSD curves for different fractal dimensions are shown in Figure 6. To simplify the process, we used uniform spherical particles in the numerical simulation and assigned uniform physical properties to the particle surfaces for study.

After model building of accumulation bodies with different fractal dimensions according to the ratios in Figure 6, we simulated the random particle accumulation process in nature using a gravitational deposition function. After gravity deposition is complete, a pressure plate is generated above the sample to compact it, simulating the tamping process in physical experiments. Following the establishment of the initial model, gravitational deposition, compaction, and gravity reduction, the accumulation model is completed, as shown in Figure 7(a). Next, the function is used to cut the sample established in the first step into a cylindrical shape, and the resulting cylindrical sample is moved to the premodelled shear box. The shear box, cylindrical sample, and upper pressure plate are then introduced into the test area, thus completing the model-building step, as shown in Figure 7(b).

Next, material assignment is carried out using the Hertz contact model. The detailed micromechanical properties used are listed in Table 2. Notably, we can set whether a group of particles has friction when in contact with other particles in MatDEM. To avoid inaccuracies caused by friction between the sample and the inner walls of the shear box, we chose to set the upper and lower shear boxes and the pressure plate as frictionless rigid bodies. Therefore, in this simulation, the normal stiffness of the shear boxes and the pressure plate is set to 10 times the normal stiffness of the sample particles, with both the normal stiffness and friction coefficient set to 0. Additionally, the energy dissipation option is enabled, and the energy loss is recorded through the aHeat matrix. The preliminary setup is complete, and the iterative simulation is ready to commence.

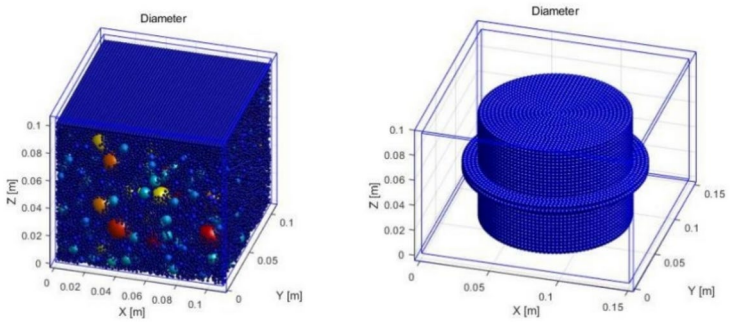

Fig. 7. Diagram of the numerical simulation experiment process: (**a**) $D = 2.5$ accumulation body, (**b**) Shear box with sample inside.

Micromechanical Properties	Normal Stiffness $k_n/(N \cdot m^{-1})$	Friction Coefficient μ	Damping
Average	1.4×10^8	0.1	0.005

Table 2. Micromechanical properties.

Complex network analysis

By modeling the particles as nodes, we are able to quantify interactions through key parameters like the average clustering coefficient, average path length, and network efficiency. This framework allows us to connect local particle behaviors to macroscopic shear properties, offering insights into the structural dynamics of large-scale accumulation bodies. For the purpose of simplifying calculations, we employed an unweighted and undirected network.

Owing to the relative displacement of particles within the shear band significantly outnumbering other parts during the shearing process, we extracted the particles within the shear band as nodes for the complex network model. According to Jiang et al.[35], the thickness of the shear band is generally between 10 d_{50} and 15 d_{50}. In this experiment, d_{50} is between 3 and 4 mm, so the shear band thickness is set to 45 mm.

In granular structures, particle contact is the most fundamental interaction at the microscopic scale. Therefore, it is crucial to quantify the overall number of contacts within the system. In complex networks, this concept is described by the degree value, where a higher average degree value indicates more particle contacts and a lower average degree value indicates fewer contacts. In addition to the node-scale information represented by the degree value, mesoscale features also play a significant role in complex networks. We introduce two parameters to describe and analyse mesoscale features: the average clustering coefficient and average path length. The average clustering coefficient measures the average ratio of actual edges to possible edges for each node in the network and describes the degree of clustering. The average path length refers to the average distance between any two points in the network, illustrating the closeness of connections between points. At the network scale, we introduce network efficiency. Network efficiency describes the average closeness and robustness of the entire network, with values ranging from 0 to 1. This reflects the efficiency of force transmission between particles and the robustness of the contact network. A higher network efficiency indicates better efficiency in force transmission between particles, less energy consumption in interactions, and superior mechanical performance of the system.

We analysed this phenomenon using the advanced complex network analysis software Pajek as a mathematical analysis tool, which aims to decipher the underlying mechanism of how the mechanical properties of the accumulation body vary with fractal dimension. Pajek offers several notable features, including speed, visualization capabilities, abstraction, and the ability to input parameters in multiple formats[36]. We utilized Pajek to model the direct shear network, enabling calculations of various complex network parameters such as degree value, clustering coefficient, average path length, and network efficiency. These calculations allow us to analyze and measure the network's structure and properties, providing insights into the importance of nodes within the network.

Results

We found a consistent pattern across different fractal dimensions. Due to space limitations, we will present detailed results only for groups 2.3, 2.5, and 2.8.

Physical experiment results

Here, we present the phenomena observed in our experiments, with a more detailed explanation provided in the subsequent sections.

Figure 8 illustrates the shear stress-shear distance relationship obtained from the large direct shear test. During the shearing process, the stress is initially redistributed among the particles, leading to a rapid and instantaneous increase in shear stress. Subsequently, as the voids between larger particles are filled and the

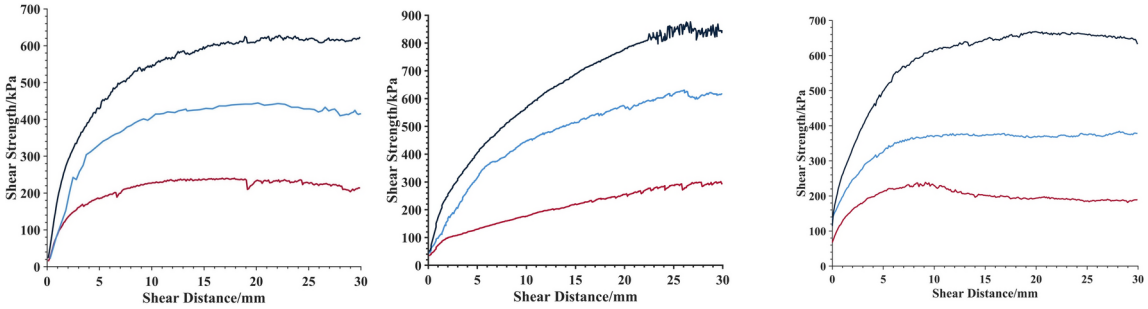

Fig. 8. Different fractal dimension shear stress-horizontal displacement relationship in physical experiment, black represents 800 kPa, blue represents 500 kPa, and red represents 200 kPa.

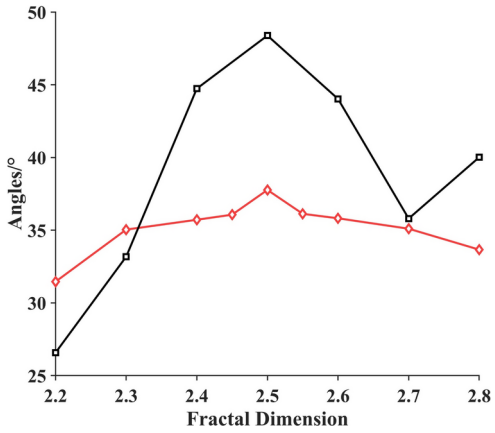

Fig. 9. Internal friction angle from the direct shear test (Black Line) and the angle of repose from static sand heap trial (Red Line).

internal structure of the particles undergoes reorganization, the specimen's resistance to deformation increases. At this stage, the shear stress continues to rise with increasing strain. After reaching the peak shear stress, the shear strength of the specimen gradually decreases and eventually stabilizes, entering the residual phase.

Figure 9 shows the variation of the internal friction angle from the direct shear test and the angle of repose from static sand heap trial with respect to the fractal dimension. When D = 2.5, they both reached maximum. These two parameters provide complementary insights into how the material's mechanical properties change with fractal dimension.

Figure 10 shows the variation in the shear strength of accumulation bodies with fractal dimension in the large direct shear test. Contrary to previous conclusions that shear strength increases with fractal dimension, the shear strength of accumulation bodies initially increases but then decreases with increasing fractal dimension, reaching its maximum at D = 2.5, following a normal distribution.

The shear strength distribution was fitted to fractal dimensions using a Gaussian distribution. The fitting results were good, as shown in Fig. 10, all conforming to $N(2.5, 0.11^2)$, and the statistical equation is provided as follows:

$$\tau = C(k + (\frac{1}{\sigma_1\sqrt{2\pi}}) \cdot e^{-\frac{(D-\mu)^2}{2\sigma_1^2}}) \tag{4}$$

where τ represents the shear strength, C is an amplification factor related to the vertical load, where $C = 11 + 0.1P$, P is the vertical load in *kPa*, k is the baseline value of the function with $k = 7$, σ_1 is the standard deviation with $\sigma_1 = 0.11$, D is the fractal dimension, and μ represents the mean value with $\mu = 2.5$.

Numerical simulation results

First, before presenting the numerical simulation results, we will verify the model's validity using data from the D=2.4 group. The results of physical experiments and numerical simulation were generally consistent as shown

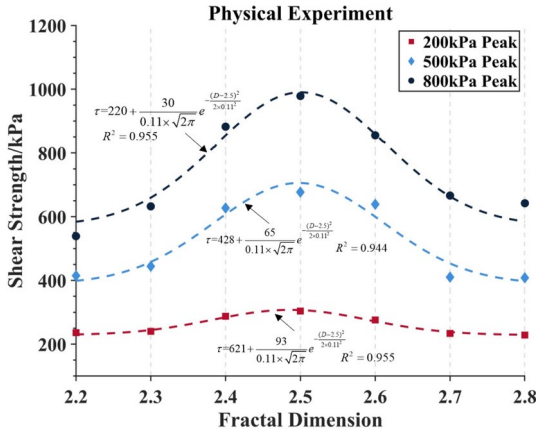

Fig. 10. The variation of shear strength with fractal dimension in the large direct shear test, with the results of normal distribution fitting under the pressure of 200 ~ 800 kPa.

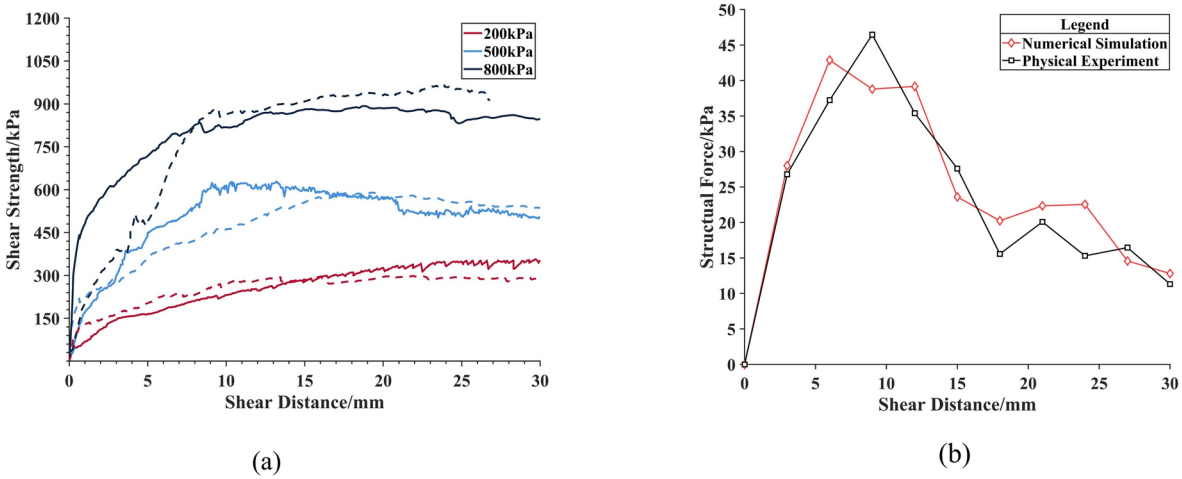

Fig. 11. Comparison between numerical simulation and physical experiment when $D=2.4$: (**a**) Stress–strain curve. The solid line represents the physical experiment, and the dashed line represents the numerical simulation result. (**b**) Comparison of structural forces between numerical simulation and physical experiment.

in Figure 11, indicating the validity of the model. When the vertical load is lower, the consistency between the numerical simulation results and physical experiment results is better than that under higher vertical loads. This is because in numerical simulation experiments, the particles are spherical, whereas in physical experiments, the particles are irregular. The irregular particles have greater friction between them. At lower vertical loads, the particles are less constrained by external forces, and the friction between particles has less of an impact on the shear strength of the sample. As the vertical load increases, the influence of friction becomes more pronounced, and the consistency decreases accordingly. The distributions of the structural forces with shear displacement obtained from the physical and numerical simulation experiments are shown in Figure 11(b), indicating that their distributions are basically similar.

The variation in shear strength with fractal dimension in the numerical simulation is shown in Fig. 12(a). The results are consistent with the results obtained from physical experiments, and the distribution of shear strength with fractal dimension also follows a normal distribution, reaching a maximum at $D=2.5$. After Gaussian distribution fitting, the shear strength obtained from the numerical simulation also follows Eq. (4), as shown in Figs. 12(b). The fitting results are promising, indicating conformity with $N(2.5, 0.085^2)$, and the statistical equation is given as follows:

$$\tau = C(k + (\frac{1}{\sigma_2\sqrt{2\pi}}) \cdot e^{-\frac{(D-\mu)^2}{2\sigma_2^2}}) \tag{5}$$

where τ represents the shear strength, C is an amplification factor related to the vertical load, where $C = 2.5 + 0.06P$, P is the vertical load in *kPa*, k is the baseline value of the function with $k = 13$, σ_2 is the

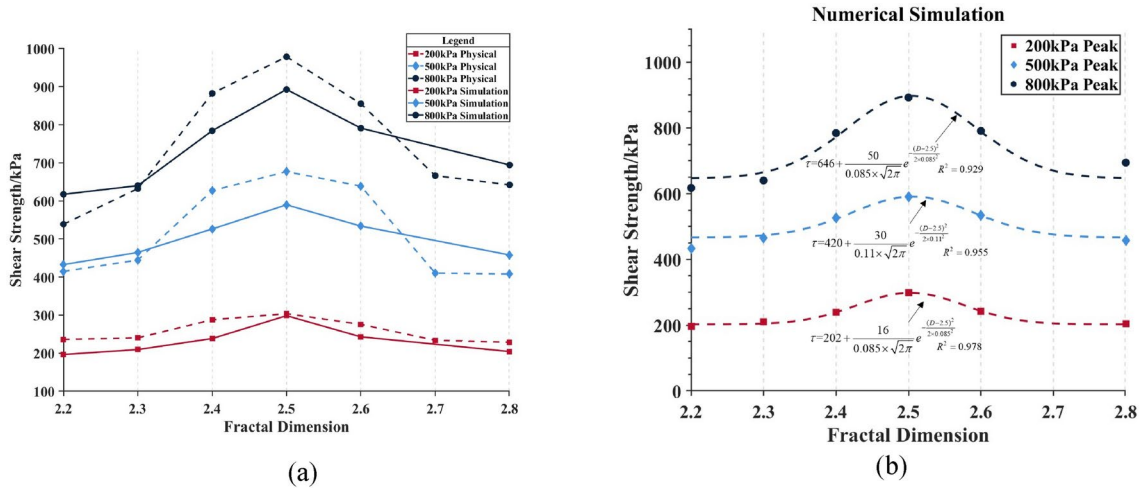

Fig. 12. The variation of shear strength with fractal dimension in numerical simulations (**a**) Comparison with physical experiments, (**b**) with the results of normal distribution fitting under the pressure of 200 ~ 800 kPa.

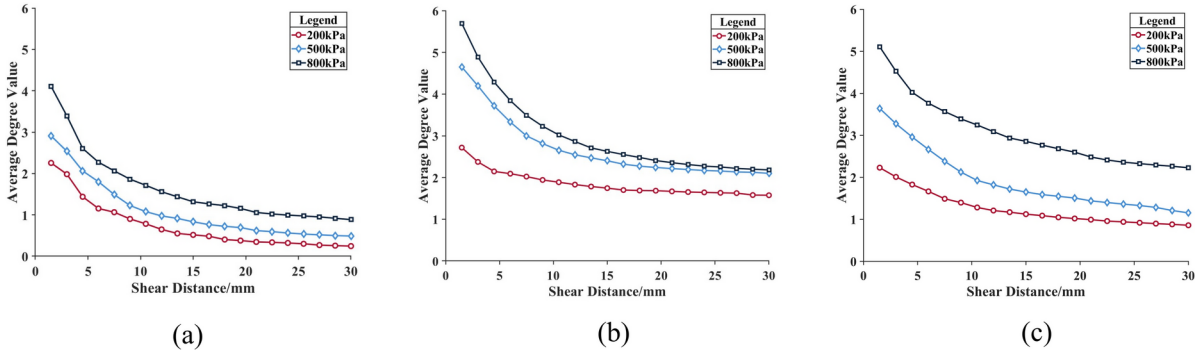

Fig. 13. Average degree value-Shear distance: (**a**) $D = 2.3$, (**b**) $D = 2.5$, (**c**) $D = 2.8$

standard deviation with $\sigma_2 = 0.085$, D is the fractal dimension, and μ represents the mean value, $\mu = 2.5$. The other parameters differ except for μ. We believe this discrepancy is due to the impossibility of numerical simulation to match physical experiments completely.

This increase-then-decrease trend in shear strength with fractal dimension obtained from both physical experiments and numerical simulations, peaking at D=2.5, suggests an optimal particle configuration that maximizes the ability to resist external deformation, which we investigate further through complex network parameters.

Complex network results

To further understand the shear strength behaviour observed in physical tests, we use complex network parameters to explore the underlying particle connectivity and force transmission, providing a microscale perspective on macroscopic strength variations. We extracted the particle data from MatDEM simulations and then calculated them in Pajek.

Average degree value

On the basis of the results of the Pajek calculations, we plotted the variation in the average degree value with shear distance, as shown in Figs. 13 (a) ~ (c). The figures show that the larger the vertical load is, the greater the average degree value for the same fractal dimension. As shear progresses, the average degree value of the network decreases. The decrease in the average degree value is particularly noticeable in the early stages of shearing. As shearing continues, the rate of decline slows, indicating that the particles are significantly reorganized during the initial shearing stage. As shearing progresses, the connections between particles gradually stabilize, and the average degree value remains stable in the later stages of shearing.

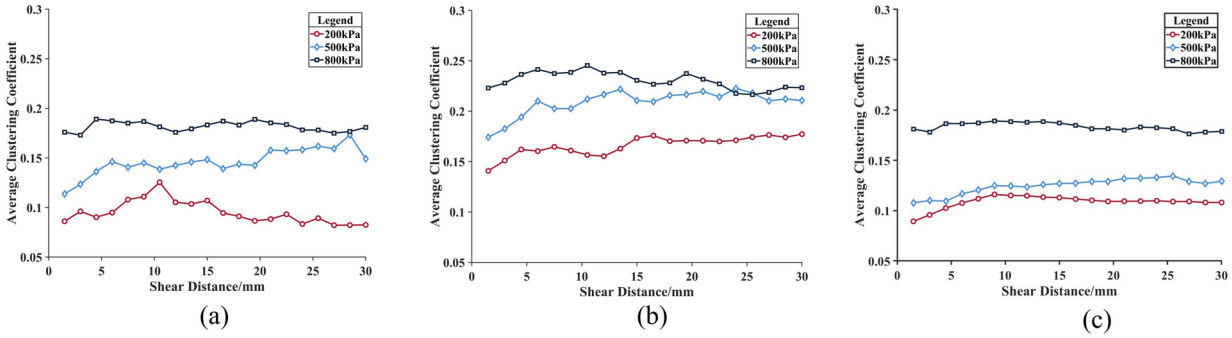

Fig. 14. Average clustering coefficient-Shear distance: (**a**) $D = 2.3$, (**b**) $D = 2.5$, (**c**) $D = 2.8$

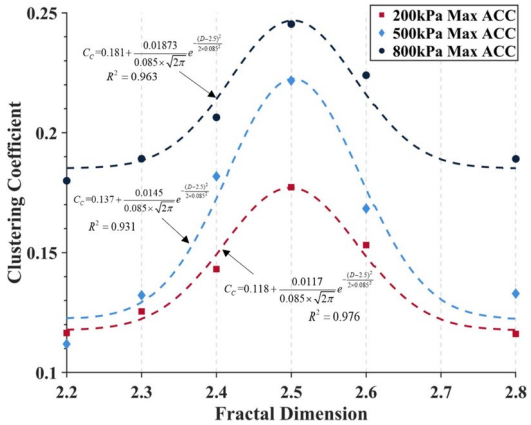

Fig. 15. Average clustering coefficient-Fractal dimension with the results of normal distribution fitting under pressure 200 ~ 800 kPa.

Average clustering coefficient

We plotted the variation in the average clustering coefficient with shear distance, as shown in Figures 14 (a)~(c). For the same fractal dimension, the average clustering coefficient of the network system increases as the vertical load increases. The average clustering coefficient does not change significantly throughout the shearing process.

Figure 15 shows the variation in the average clustering coefficient of accumulation bodies with fractal dimension in the large direct shear test. The high clustering coefficient at $D = 2.5$ indicates a densely interconnected particle network, which correlates with the peak shear strength observed, suggesting that denser particle connections improve stability. The clustering coefficient distribution with fractal dimensions was statistically analysed and fitted using a Gaussian distribution. The results, shown in Fig. 15, indicate a good fit, all of which conform to $N(2.5, 0.085^2)$, and the following statistical equation is provided:

$$C_C = C(k + (\frac{1}{\sigma_3\sqrt{2\pi}}) \cdot e^{-\frac{(D-\mu)^2}{2\sigma_3^2}}) \tag{6}$$

where C_c is the clustering coefficient, C is an amplification factor related to the vertical load, $C = 0.0093 + 0.00001P$, P is the vertical load in *kPa*, k is the baseline value of the function, $k = 10$, σ_3 is the standard deviation, $\sigma_3 = 0.085$, D is the fractal dimension, and μ is the mean value, $\mu = 2.5$. Comparing Eq. (5) and Eq. (6), we find that in the numerical simulation, the macroscopic parameter (shear strength) and the microscopic parameter (average clustering coefficient) both conform to a similar normal distribution, indicating that changes in the microscopic complex network parameters can explain changes in the macroscopic mechanical properties of the accumulation body.

Average path length

Figure 16 (a)~(c) shows the variation in the average path length with shear distance under different vertical loads. The figure reveals that the greater the vertical load is, the shorter the average path length for the same fractal dimension, which indicates a denser particle contact network and a stronger structure. Its trend with

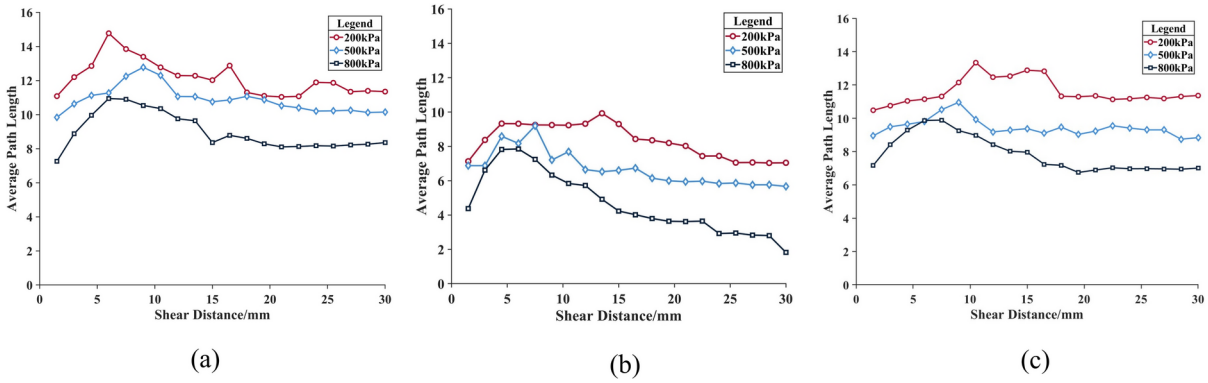

Fig. 16. Average path length: (**a**) $D = 2.3$, (**b**) $D = 2.5$, (**c**) $D = 2.8$

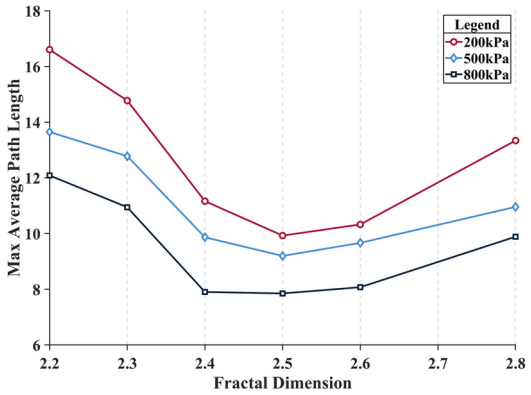

Fig. 17. Maximum average path length for different fractal dimensions.

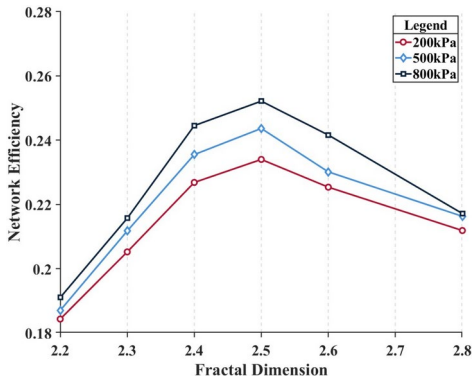

Fig. 18. Network efficiency for different fractal dimensions.

changing vertical load is opposite to that of the average clustering coefficient, which is consistent with the theory of complex networks, i.e., the more closely the network is connected, the larger the average clustering coefficient, and, correspondingly, the shorter the average path length.

Figure 17 shows that under the same vertical load, the distribution of the average path length with fractal dimension is opposite to that of the average clustering coefficient. This further indicates that when the fractal dimension $D = 2.5$, the overall network is the most robust, and the particle connections are the tightest, which is consistent with the mechanical performance results from the physical experiments.

Network efficiency

Using MATLAB software, we computed the network efficiency for different fractal dimensions under various vertical loads. The results are shown in Figure 18. The results indicate that network efficiency increases with

vertical load; for the same vertical load, network efficiency follows a bell-shaped curve concerning the fractal dimension. The bell-shaped trend in network efficiency, with a peak at D=2.5, aligns with the Gaussian pattern observed in shear strength, indicating that the most efficient force transmission occurs at this fractal dimension, enhancing stability.

From the analysis of the average clustering coefficient, average path length, and network efficiency, we concluded that the network of the accumulation body first strengthens and then weakens with increasing fractal dimension. At D=2.5, clustering is most pronounced, connections are tightest, and network efficiency reaches its peak, indicating that the network achieves its most robust state. This interpretation offers a microscale perspective on the phenomenon observed in physical experiments where the shear mechanical properties initially strengthen and then weaken with increasing fractal dimension.

Conclusions

Owing to the complexity of large-scale accumulation bodies, understanding their mechanical properties from the perspective of granular materials remains a challenging and interesting topic in geotechnical engineering. This study aims to investigate the relationship between the particle fabric characteristics of accumulation bodies and their shear mechanical properties. We employed fractal dimensions to describe the fabric features of these accumulation bodies and conducted large direct shear tests as well as discrete element method simulations based on MatDEM under various vertical loads. On the basis of the experimental results, this research enhances the comprehension of how fabric characteristics affect the macroscopic mechanical behaviour of granular materials, which not only offers a scientific basis for the optimal mix design of artificial construction materials but also introduces a new approach for evaluating the stability of large-scale accumulation bodies, the main conclusions are as follows:

1) Unlike previous conclusions that the shear strength of accumulation body increases with increasing fractal dimension, under the same vertical load, both the shear strength obtained from physical tests and numerical simulations and the internal friction angle initially increase and then decrease as the fractal dimension increases, the maximum values are observed when the fractal dimension D = 2.5. Statistical formulas for the variation in shear strength with fractal dimension is provided, all following a normal distribution with a mean value of 2.5 and an amplification factor that is proportional to the vertical load.
2) We calculated complex network parameters, observed that as vertical load increases, the average degree of particles rises, the average clustering coefficient increases, and the average path length decreases; the network efficiency initially increases and then decreases with increasing fractal dimension, peaking at D = 2.5, while the average path length exhibits the opposite trend. The analysis of these complex network parameters offers a fresh perspective on the mechanisms driving the observed patterns in physical experiments and numerical simulations of particle contact network.
3) It is worth noting that the average clustering coefficient follows a normal distribution nearly consistent to that observed in the numerical simulation experiments, with the same mean value of 2.5, same standard deviation of 0.085 and an amplification factor that is proportional to the vertical load. These physical quantities above obtained consistent patterns of how the fractal dimensions influenced on the mechanical properties of granular materials from various perspectives, providing a new interpretation of the mechanisms by which fractal dimensions affected their shear characteristics from the perspective of the topological structure of the particle contact network.

Last but not least, considering the significant variation in the particle size within each sample, the changes in the void ratio and expansion behaviour during shearing remain to be studied, and further insights can be gained as new testing and analysis methods become available.

Data availability

All data, models, and code generated or used during the study appear in the submitted manuscript.

Received: 20 October 2024; Accepted: 12 February 2025
Published online: 06 March 2025

References

1. Xu, W. J. & Hu, R. L. Conception, classification and significations of soil-rock mixture. *Hydrogeol. Eng. Geol.* **36**(04), 50–56 (2009) (**in Chinese**).
2. Liu, H. Q. & Hu, R. L. Coupling of earth's endogenic and exogenic geological processes on formation mechanism of large-scale loose complex quaternary deposits in western China. *J. Eng. Geol.* **16**(3), 291–297 (2008) (**in Chinese**).
3. Zhang, Y. et al. Effects of fractal dimension and water content on the shear strength of red soil in the hilly granitic region of southern China. *GEOMORPHOLOGY* **351**, 106956 (2020).
4. Jia, J. Q. et al. Dynamic stability analysis method of anchored rocky slope considering seismic deterioration effect. *Sci. Rep.* **14**(1), 1–22 (2024).
5. Yao, L. K., Li, S. X. & Jiang, L. W. Self-organized criticality and its application in granular mixtures. *J. Sichuan Univ. (Eng. Sci. Edit.)* **35**(1), 8–14 (2003).
6. Baxter, J., Tüzün, U., Heyes, D., Hayati, I. & Fredlund, P. Stratification in poured granular heaps. *Nature* **391**, 136. https://doi.org/10.1038/34328 (1998).
7. Huang, Y. D. & Yao, L. K. Size distribution law of earthquake-triggered landslides in different seismic intensity zones. *NONLINEAR PROCESS. GEOPHYS.* **28**(1), 167–179 (2021).
8. Xiao, J. Z. et al. Cracking mechanism of secondary lining for a shallow and asymmetrically-loaded tunnel in loose deposits. *Tunn. Undergr. Space Technol.* **43**(232), 240 (2014).

9. Duan, S. Q. et al. Mechanical response and data-driven fatigue model of interlayer soils in track-bed considering multi-factor coupling effect. *Comput Geotech.* **163**, 105749 (2023).
10. Duan, S. Q. et al. A new perspective on the semi-quantitative meso-structural failure mechanism of deep weak interlayer zone under different stress paths. *Rock Mech. Rock Eng.* **57**, 3171–3195 (2024).
11. Zhao, J. S. et al. Failure mechanism of rock masses with complex geological conditions in a large underground cavern: A case study. *Soil Dyn. Earthq. Eng.* **177**, 108439 (2024).
12. Zhao, J. S. et al. Rock fracturing observation based on microseismic monitoring and borehole imaging: In situ investigation in a large underground cavern under high geostress. *Tunn. Undergr. Space Technol.* **126**, 104549 (2022).
13. General Administration of Quality Supervision, Inspection and Quarantine of the People's Republic of China, & Standardization Administration of China. *Standard for engineering classification of soil (GB 50145–2017)* (China Standards Press, 2017).
14. Su, Y., Cui, Y. J., Dupla, J. C. & Canou, J. Experimental investigation and modelling of the mechanical behaviors of fine/coarse soil mixture. *Transp. Geotech.* **49**, 101382 (2024).
15. Su, Y., Cui, Y. J., Dupla, J. C. & Canou, J. Soil-water retention behaviour of fine/coarse soil mixture with varying coarse grain contents and fine soil dry densities. *Can. Geotech. J.* **59**(2), 291–299 (2022).
16. Hartmann, D. & Christiansen, C. Settling velocity distributions and sorting processes on a longitudinal dune: A case study. *Earth Surf. Process. Landf.* **13**(7), 649–656 (1988).
17. Perfect, E. & Kay, B. D. Fractal theory applied to soil aggregation. *Soil Sci. Soc. Am. J.* **55**(6), 1552–1558 (1991).
18. Hwang, S. I. & Powers, S. E. Using particle-size distribution models to estimate soil hydraulic properties. *Soil Sci. Soc. Am. J.* **67**(4), 1103–1112 (2003).
19. Su, Y., Cui, Y. J., Dupla, J. C. & Canou, J. Effect of water content on permanent deformation of fine/coarse soil mixtures with varying coarse grain contents and subjected to multi-stage cyclic loading. *Acta Geotech.* **17**(8), 3259–3268 (2022).
20. Turcotte, D. L. Fractals and fragmentation. *J. Geophys. Res.: Solid Earth* **91**(B2), 1921–1926 (1986).
21. Chen, G. et al. Experimental study on mechanical strength and acoustic emission characteristics of waste rock cemented backfill. *Bull. ENG. GEOL. ENVIRON.* **83**(4), 1–13 (2024).
22. Zhang, W. et al. Stability evaluation and potential failure process of rock slopes characterized by non-persistent fractures. *Nat. Hazard. Earth Syst. Sci.* **20**(11), 2921–2935 (2020).
23. Avşar, E. Contribution of fractal dimension theory into the uniaxial compressive strength prediction of a volcanic welded bimrock. *Bull. Eng. Geol. Environ.* **79**(7), 3605–3619 (2020).
24. Jaeger, H. M., Nagel, S. R. & Behringer, R. P. Granular solids, liquids, and gases. *Rev. Mod. Phys.* **68**(4), 1259–1273 (1996).
25. Sun, Q. C., Liu, X. X., Zhang, G. H., Liu, C. Q. & Jin, F. The mesoscopic structures of dense granular materials. *Adv. Mech.* **47**(1), 263–308 (2017) (**in Chinese**).
26. Walker, D. M. & Tordesillas, A. Topological evolution in dense granular materials: A complex networks perspective. *Int. J. Solids Struct.* **47**(5), 624–639 (2010).
27. Walker, D. M., Tordesillas, A., Einav, I. & Small, M. Complex networks in confined comminution. *Phys. Rev. E.* https://doi.org/10.1103/PhysRevE.84.021301 (2011).
28. Tordesillas, A., Walker, D. M., Ando, E. & Viggiani, G. Revisiting localized deformation in sand with complex systems. *Proc. R. soc. A-Math. Phys. Eng. Sci.* **469**(2152), 20120606 (2013).
29. Li, Z.Q. *Numerical simulation of topological mechanics of particle force chain network based on complex network theory*. Dissertation, Xiangtan University (In Chinese) (2017).
30. Yang, P. L., Luo, Y. P. & Shi, Y. C. Soil fractal characteristics characterized by weight distribution of particle size. *Chin Sci. Bull.* **20**, 1896–1899 (1993) (**In Chinese**).
31. Sun, K. C. et al. Experimental research on the influence of particle size and gradation on repose angle of rockfill. *J. Changjiang River Sci. Res. Inst.* **33**(8), 91–95 (2016) (**in Chinese**).
32. Cundall, P. A. A computer model for simulating progressive, large-scale movement in blocky rock system. *Proc. Int. Symp. Rock Mech.* **8**(129), 136 (1971).
33. Cundall, P.A. *The Measurement and Analysis of Accelerations in Rock Slopes.* (University of London, 1971)
34. Liu, C. *Matrix Discrete Element Analysis of Geology and Geotechnical Engineering* (Science Press, 2019) (**in Chinese**).
35. Jiang, M. J., Wang, F. Z., Zhu, H. H., Hu, H. J. & Zhao, T. DEM simulation of macro-micro mechanical properties of dense granular materials in direct shear test. *J. Hohai Univ. (Nat. Sci.)* **38**(5), 538–544 (2010) (**in Chinese**).
36. Xie, CK. *Analysis of instability problem of cohesive soil particle accumulation based on complex network*. Dissertation, Xiangtan University (2019)

Acknowledgements

We would like to extend our sincerest gratitude to Gan Jiewei and Chen Qifeng for their advice and support in the research.

Author contributions

Y.D.H.: Review & Editing, Supervision, Conceptualization, Funding acquisition, Project administration, Resources, Validation, Methodology, Data curation. W.T.C.: Original draft, Data curation, Formal analysis, Methodology, Software, Visualization, Investigation.

Funding

National Natural Science Foundation of China,52378466,The Tibet Autonomous Region Science and Technology Department 2024 Major Science and Technology Project,XZ202402ZD0003

Declarations

Competing interests

The authors declare no competing interests.

Additional information

Supplementary Information The online version contains supplementary material available at https://doi.org/10.1038/s41598-025-90293-9.

Correspondence and requests for materials should be addressed to Y.H.

Reprints and permissions information is available at www.nature.com/reprints.